Letters on Materials 9 (4), 2019 pp. 475-479 www.lettersonmaterials.com

https://doi.org/10.22226/2410-3535-2019-4-475-479 PACS: 61.46.+w, 75.50.Bb, 75.60.-d

Effect of the Red/Ox ratio on the structure and magnetic behavior of $Li_{0.5}Fe_{2.5}O_4$ nanocrystals synthesized by solution combustion approach

K. D. Martinson[†,1], I. B. Panteleev[2], A. P. Shevchik[2], V. I. Popkov[1]

[†]martinsonkirill@mail.ru

[1]Ioffe Physical-Technical Institute of the RAS, 26 Politeknicheskaya St., St. Petersburg, 194021, Russia
[2]Saint Petersburg State Institute of Technology, 26 Moskovsky Av., St. Petersburg, 190013, Russia

In this research, nanocrystalline lithium ferrite ($Li_{0.5}Fe_{2.5}O_4$) was synthesized using the solution combustion approach with using glycine as fuel and a chelating agent at various Red/Ox ratios ("glycine to nitrate" ratio $G/N = 0.4, 0.6, 0.8, 1.0$). According to the data of energy-dispersive X-ray spectroscopy (EDX) and atomic absorption spectroscopy (AAS), the prepared samples correspond in their composition to stoichiometric ferrite $Li_{0.5}Fe_{2.5}O_4$ within the error of the determination methods used. The results of powder X-ray diffractometry (PXRD) confirmed the formation of α-$Li_{0.5}Fe_{2.5}O_4$ at G/N ratio of 0.8 and 1.0 and the presence of β-$Li_{0.5}Fe_{2.5}O_4$ modification in case of deficiency ($G/N = 0.4$) and stoichiometry ($G/N = 0.6$) of the chelating agent. It is shown that a change in the Red/Ox composition of reacting solutions affects not only the phase composition of the synthesized lithium ferrite samples, but also the crystallite size, which lies in the range from 22 to 35 nm. Based on the scanning electron microscopy (SEM) data, it was found that $Li_{0.5}Fe_{2.5}O_4$ powders had a developed porous microstructure consisting of micron agglomerates. According to the vibration magnetometry data of nanocrystalline lithium ferrite powders, it follows that all synthesized compositions have a pronounced ferrimagnetic behavior, despite the presence of β-modification in some of them. It is shown that by varying the Red/Ox environment and, as a consequence, the phase composition and crystallite size, it is possible to obtain $Li_{0.5}Fe_{2.5}O_4$ nanocrystals with magnetic parameters in the following ranges: saturation magnetization (M_s) = 51.6 – 61.9 emu/g, residual magnetization (M_r) = 14.3 – 17.8 emu/g, coercive force (H_c) = 109 – 135 Oe.

Keywords: solution combustion synthesis, lithium ferrite, nanocrystals, magnetic materials, ferrimagnets.

1. Introduction

Due to its outstanding electrical and magnetic properties, lithium ferrite ($Li_{0.5}Fe_{2.5}O_4$) has found wide applications in various fields of modern industry [1–3]. High saturation magnetization values, low dielectric loss, high Curie temperature, low coercive force, low cost, and high chemical stability make it one of the most popular materials in the production of different microwave devices with a wide range of applications [4 – 7]. Besides, the active development of new fields of using nanostructured lithium ferrite, for example, as an anode material in lithium-ion batteries, magnetic fluids, biomedicine, is currently underway [8 –10].

The electromagnetic parameters of ferrites depend on many factors, such as the presence of additional M^{2+} cations in the spinel structure (Co, Ni, Zn, Mn, Mg), crystallite size, microstructure and morphology [11–13]. All of the above factors are directly dependent on the technology of obtaining both the initial pre-ceramic powder and the temperature conditions of sintering of the final ceramic product [14]. In industry, lithium ferrites usually are prepared via a solid-state reaction by sintering at fairly high temperatures (1000 –1100°C) [15]. However, losses of lithium and oxygen during sintering have a negative effect on the electromagnetic parameters of the resulting compositions [16]. One of the possible solutions to this problem is the transition to "wet chemistry" methods that can not only improve the stability of the functional properties of ceramics from lithium ferrites, but also obtain the initial pre-ceramic powders in the nanometer range. At present, a large number of methods for producing nanostructured ferrites are known, for example, sol-gel synthesis, hydrothermal synthesis, sonochemical method, plasma-chemical synthesis, etc. [17 – 22]. One of the increasingly popular methods is the synthesis of ferrites under solution combustion conditions, which, due to the possibility of controlling the structural parameters and morphology of the resulting compositions, allows one to obtain nanostructured ferrites in a wide range of crystallite sizes [23]. Besides, a large number of works aimed at the development of installations for the continuous synthesis of nanopowders by the solution combustion method make this method popular in industry [24]. However, the development of technologies for the production of microwave ceramics based on lithium ferrites obtained by the solution combustion method is impossible without studying the effect of the Red/Ox environment on the structure and magnetic characteristics of the resulting compositions.

In the present work, we report on the role of the Red/Ox ratio in the structure and magnetic behavior of nanostructured lithium ferrite. All prepared samples of $Li_{0.5}Fe_{2.5}O_4$ were comprehensively analyzed, including determination of chemical composition, morphology, crystal structure, and magnetic parameters. Also, the unit cell parameters and structural parameters of the prepared compositions were refined.

2. Materials and methods

Nanocrystalline lithium ferrite was obtained by the solution combustion method using glycine as fuel at various Red/Ox ratios in the reaction mixture (G/N=0.4, 0.6, 0.8, 1.0). The initial reagents $Fe(NO_3)_3 \cdot 9H_2O$ (puris.) (NevaReactiv, Russia), $LiNO_3 \cdot 3H_2O$ (puris.) (NevaReactiv, Russia) and $C_2H_5NO_2$ (puris.) (NevaReactiv, Russia) were dissolved in 50 ml of distilled water with 3M HNO_3 added while heating the solution to 50°C. The number of reagents was calculated based on the reaction of glycine-nitrate combustion:

$$LiNO_3 + 5Fe(NO_3)_3 + 40/9C_2H_5NO_2 = \\ = 2Li_{0.5}Fe_{2.5}O_4 + 80/9CO_2\uparrow + 56/9N_2\uparrow + 316/9H_2O\uparrow. \quad (1)$$

The reaction solution prepared in this way was mixed for 20 minutes until the reagents were completely dissolved. After homogenization, the solutions were heated to the self-ignition point, which was achieved with almost complete evaporation of water, and then resulting brown powders were formed. The prepared samples were thermally treated in a muffle furnace at a temperature of 500°C for 2 hours to remove impurity organics. The resulting powders were mechanically milled in a mortar.

The chemical composition and morphology were investigated using a Tescan Vega 3 SBN scanning electron microscope equipped with an Oxford INCA x-act x-rat spectral microanalysis device and an AA-7000 atomic absorption spectrometer. Phase evolution was analyzed by a Rigaku SmartLab 3 powder diffractometer using monochromatic $Cu_{K\alpha}$ radiation and ICDD PDF-2 powder database. The structural parameters and unit cell values were refined by the Rietveld method using Rigaku SmartLab Studio software. The average crystallite size (coherent scattering area) was determined from the X-ray diffraction lines broadening using the Scherrer equation:

$$D = \frac{k \cdot \lambda}{\beta \cdot \cos\theta} \quad (2)$$

where k is the crystal shape factor (assumed to be 0.94 in the isometric approximation), λ is the X-ray emission wavelength ($Cu_{K\alpha}$, λ=0.15406 nm), β is the diffraction maximum broadening with considering instrumental error (in radians), θ is the diffraction peak position (Bragg angle).

The pycnometry density of the obtained samples was determined by gas pycnometry (helium). It was carried out using an UltraPyc 1200 pycnometer (QuantaChrome, USA) in 1 cm^3 microcell through degassing the samples in a helium flow (degassing time 10 minutes, 10 consecutive measurements). The magnetic parameters of nanocrystalline $Li_{0.5}Fe_{2.5}O_4$ were measured using a Lake Shore 7410 vibration magnetometer at 298 K with magnetization (M) vs magnetic field (H) mode.

3. Results and discussion

According to X-ray diffractometry data, the combusted powders are single-phase lithium ferrite (JCPDS card #38–0259) with a spinel structure in two different modifications α-$Li_{0.5}Fe_{2.5}O_4$ (space group $P4_332$) and β-$Li_{0.5}Fe_{2.5}O_4$ (space group Fd_3m) (Fig. 1). The obtained data show that with a small excess of fuel (G/N=0.8), an ordered alpha phase of lithium ferrite is formed (≈93%), with a small amount of β disordered modification. In the case of deficiency (G/N=0.4) and excess (G/N=1.0) of glycine, a significant increase in beta modification of lithium ferrite is observed (up to 30–40%), which may be due to the mechanism of lithium ferrite formation via the solution combustion synthesis, which is discussed below.

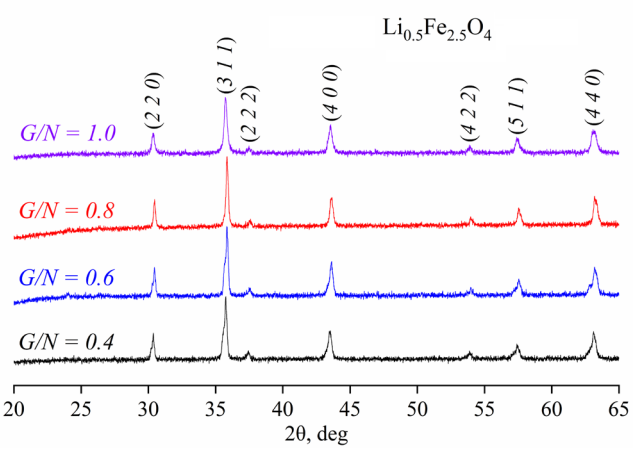

Fig. 1. (Color online) X-ray diffraction patterns for nanocrystalline lithium ferrite obtained via solution combustion method.

It is known that by varying the Red/Ox composition of the reaction mixture, it is possible to control the type of combustion and synthesis temperature, composition, morphology, microstructure and electromagnetic parameters of the resulting combustion products [25]. In turn, a change in the redox environment is possible both by choosing various types of reducing agents (glycine, urea, citric acid, etc.) and oxidizing agents (nitrates, perchlorates, oxalates), and by varying the amount of fuel involved in the reaction [26]. At a stoichiometric ratio of the oxidizing agent to the reducing agent (G/N=0.6), the oxidation proceeds completely without atmospheric oxygen, whereas in the case of excess (G/N>0.6) or lack of fuel (G/N<0.6), it takes an active part in the process. In work [22] Naderi et al. found that the adiabatic temperature of the combustion flame in process of the lithium ferrite formation using glycine as a fuel at a stoichiometric ratio is 2332°C and, when G/N deviates from stoichiometry, it can decrease to 500°C. However, the stoichiometry point is usually biased towards a small excess of fuel (G/N=0.8), and the actual temperature during combustion is much lower. This change in temperature directly affects the phase evolution of the resulting product and explains the presence of a disordered β modification of lithium ferrite in samples obtained with a significant lack of fuel. This modification has a disordered face-centered cubic structure where Li^+ and Fe^{3+} cations randomly distributed over the octahedral sites. In the

case of solid-state methods for producing lithium ferrites, the transition from α-$Li_{0.5}Fe_{2.5}O_4$ to β-$Li_{0.5}Fe_{2.5}O_4$ occurs in the temperature range from 730 to 760°C [27], however, in the case of glycine-nitrate combustion, the reaction temperature during stoichiometry is much higher, but the transition from alpha to beta does not occur.

Besides, Rietveld refining of the nanocrystalline lithium ferrite alpha and beta modifications confirms the change in the unit cell parameters with a change in Red/Ox ratio, which is seen in the given diffraction patterns. The details of the crystal data and the selected crystallographic parameters are presented in Table 1. The lattice parameters of lithium ferrite obtained at a stoichiometric ratio of glycine to nitrogen in nitrates (a = 8.324(4) Å) are in good agreement with the reported values of α-$Li_{0.5}Fe_{2.5}O_4$ [28]. In other samples, it was determined that the lattice parameters of the prepared lithium ferrite powders are quite lower (a = 8.290(2) Å). The obtained values are also in good agreement with the unit cell parameters of the β-$Li_{0.5}Fe_{2.5}O_4$ given in the literature [27]. Furthermore the pycnometric density data of the obtained lithium ferrite samples at non-stoichiometric Red/Ox ratios also indirectly confirm the presence of a disordered modification, whose density value is lower (4.421 g/cm^3) than that of the alpha modification (4.591 g/cm^3), which is also consistent with previously published data [29].

Table 1. Structural data and Rietveld refinement results of α- and β-$Li_{0.5}Fe_{2.5}O_4$.

Structural modification	α-$Li_{0.5}Fe_{2.5}O_4$	β-$Li_{0.5}Fe_{2.5}O_4$
Space group	$P4_332$	Fd-3m
a (Å)	8.324(4)	8.290(2)
V (Å^3)	576.761(73)	569.722(11)
ρ, g/cm^3	4.591	4.421
R_p, %	2.65	2.78
R_{wp}, %	3.14	3.04
χ^2	2.47	2.41

Based on the X-ray diffraction lines broadening and the Scherrer equation, the average crystallite size of $Li_{0.5}Fe_{2.5}O_4$ was found to be from 22 ± 2 to 35 ± 4 nm, depending on the Red/Ox ratio. The largest crystallite sizes are observed for the samples obtained at a ratio of G/N = 0.6 and 0.8 and are 31 and 35 nm, respectively. When the Red/Ox ratio is shifted toward excess and deficiency, a slight decrease in crystallite sizes is observed up to 22 nm in the case of fuel lack and up to 24 nm in the case of fuel excess. Such changes are also associated with the nanocrystals formation temperature and are described in detail in previous works [13, 23].

The morphology and composition of nanostructured lithium ferrite powders synthesized via the solution combustion method were investigated by scanning electron microscopy, energy-dispersive X-ray spectroscopy, and atomic absorption spectroscopy. According to the obtained data, the composition of the synthesized samples on the main components — lithium (Li) and iron (Fe) is 25 and 85 at.% respectively, which corresponds to lithium ferrite stoichiometry within the error of the determination method. Slight deviations within 1.5% of the calculated composition are observed for the sample synthesized at a ratio of G/N = 0.4, which is associated with a significant deviation from stoichiometry and smoldering combustion mode. The SEM micrographs show the effect of the Red/Ox environment on the morphology of the obtained lithium ferrite powders (Fig. 2). It is noticeable that the samples synthesized at a ratio of G/N = 0.6 and 0.8 have a developed porous microstructure typical of ferrites obtained by solution combustion method and are associated with abundant gas evolution during the combustion process [11]. The difference in the morphology of the samples synthesized with a deficiency and excess of a reducing agent is associated with the temperature combustion mode.

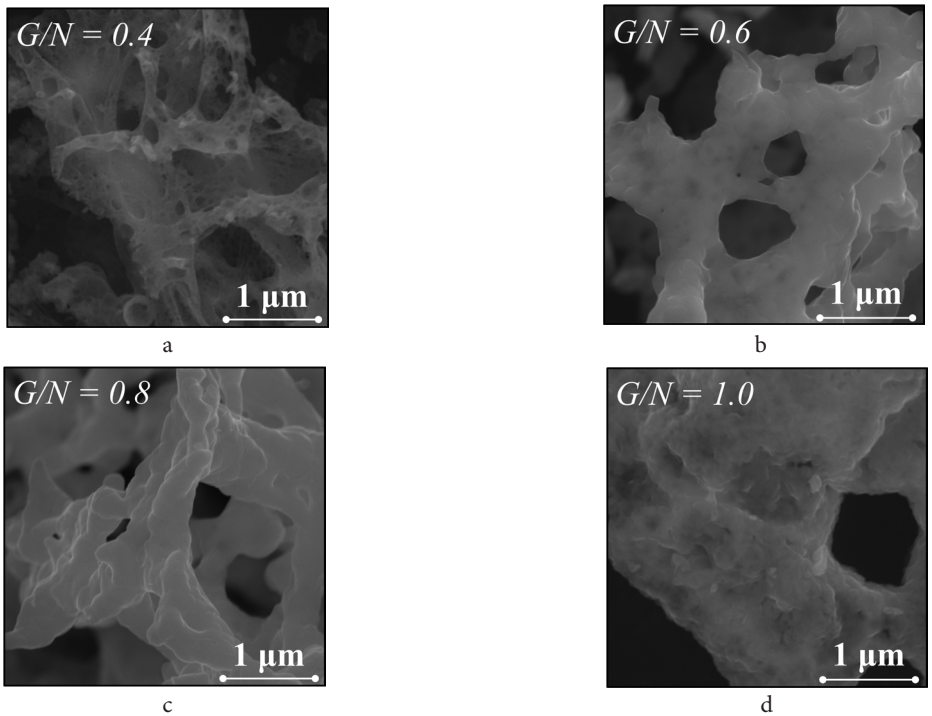

Fig. 2. SEM micrographs for lithium ferrite powders synthesized at different Red/Ox ratios: G/N = 0.4 (a), G/N = 0.6 (b), G/N = 0.8 (c), G/N = 1.0 (d).

Fig. 3 shows the hysteresis loops of nanocrystalline lithium ferrite synthesized via the glycine-nitrate combustion method at different G/N ratios. All prepared samples demonstrate a ferrimagnetic behavior with high saturation magnetization values and a small coercive force. The highest values of saturation magnetization (M_s=61.0 emu/g), residual magnetization (M_r=17.8 emu/g), and coercive force (H_c=135 Oe) are observed for the sample synthesized at a ratio of 0.8, which is associated with the highest percentage of the ordered phase in its composition. It is known that nanocrystalline β-$Li_{0.5}Fe_{2.5}O_4$ has a similar magnetic behavior as the α-$Li_{0.5}Fe_{2.5}O_4$, which explains the similarity of the appearance of the hysteresis loops in all synthesized samples, despite the presence of a disordered modification in some of them [30]. However, the magnetic properties of spinel ferrites strongly depend not only on the phase composition but also on the crystallite size, microstructure, and cation distribution. These factors explain the difference in the magnetic characteristics of lithium ferrite obtained at various Red/Ox ratios.

The summarized results of the magnetic characteristics are presented in Fig. 4. The data indicate that depending on the phase composition, crystallite size and morphology of lithium ferrite obtained under conditions of glycine nitrate, the magnetic characteristics range from 61.9 to 51.6 emu/g in the case of saturation magnetization, from 14.3 to 17.8 emu/g for residual magnetization and from 109 to 135 Oe for coercive force. The lowest values of magnetic characteristics are observed for the sample synthesized with a significant lack of glycine and with the highest content of disordered β-modification.

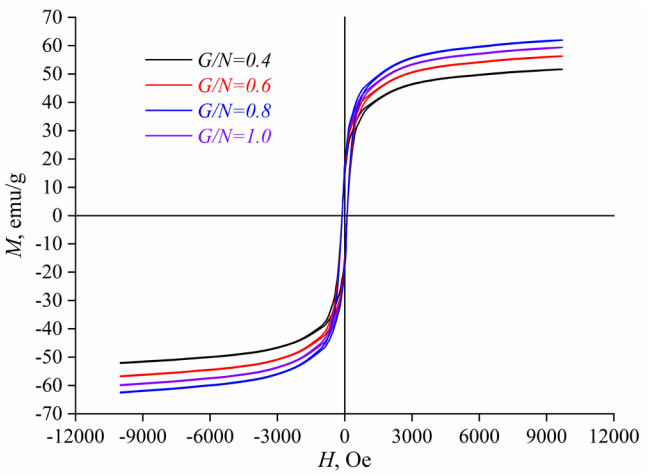

Fig. 3. (Color online) Hysteresis loops of lithium ferrite powders prepared via solution combustion approach.

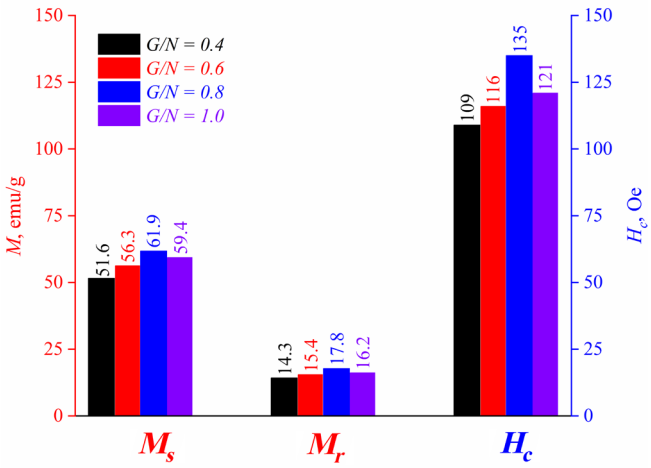

Fig. 4. (Color online) The saturation magnetization (M_s), residual magnetization (M_r) and coercivity force (H_c) of nanocrystalline $Li_{0.5}Fe_{2.5}O_4$ samples obtained by solution combustion method.

4. Conclusions

Nanostructured lithium ferrite powders were obtained via the solution combustion method using glycine as a fuel, with a crystallite size in the range from 22 to 35 nm. The effect of the Red/Ox behavior on the phase composition, crystallite size, morphology, and magnetic characteristics was shown. It was established that an almost pure ordered phase of α-$Li_{0.5}Fe_{2.5}O_4$ was formed in the stoichiometric ratio of glycine to nitrogen in nitrates, while disordered β-$Li_{0.5}Fe_{2.5}O_4$ appeared with a shortage and excess of fuel. The residual magnetization (M_r), saturation magnetization (M_s) and coercive force (H_c) of the synthesized nanocrystalline $Li_{0.5}Fe_{2.5}O_4$ also depend on the G/N ratio and change in following range: M_s=61.9–51.6 emu/g, M_r=14.3–17.8 emu/g and H_c=109–135 Oe.

References

1. G.R. Rao, B.L. Rekha, K.N. C. Kumar, C.A. Kumar, K. Samatha, M.P. Dasari. Journal of Magnetism and Magnetic Materials. 444, 444 (2017). Crossref
2. G.R. Gajula, L.R. Buddiga, N. Vattikunta. Materials Chemistry and Physics. 230, 331 (2019). Crossref
3. M. Usakova, E. Usak, R. Dosoudil, J. Kruzelak. AIP Conference Proceedings. 2131, 020049 (2019). Crossref
4. S.S. Teixeira, M.P. F. Graca, L.C. Costa. Spectroscopy Letters. 47 (5), 356 (2014). Crossref
5. N. Rezlescu, C. Doroftei, E. Rezlescu, P.D. Popa. Sensors and Actuators B: Chemical. 133 (2), 420 (2008). Crossref
6. M.M. Costa, R.S.T.M. Sohn, A.A.M. Macedo, S.E. Mazzetto, M.P.F. Graca, A.S.B. Sombra. Journal of Alloys and Compounds. 509, 9466 (2011). Crossref
7. R.S.T.M. Sohn, A.A.M. Macedo, M.M. Costa, S.E. Mazzetto, A.S.B. Sombra. Physica Scripta. 82 (5), 055702 (2010). Crossref
8. V.K. Sankaranarayanan, O. Prakash, R.P. Pant, M. Islam. Journal of Magnetism and Magnetic Materials. 252, 7 (2002). Crossref
9. H. Zeng, T. Tao, Y. Wu, W. Qi, C. Kuang, S. Zhou, Y. Chen. RSC Advances. 44 (4), 23145 (2014). Crossref
10. M. Dasari, G.R. Gajula, D.H. Rao, A.K. Chintabathini, S. Kurimella, B. Somayajula. Processing and Application of Ceramics. 11 (1), 7 (2017). Crossref
11. S.V. Dyachenko, K.D. Martinson, I.A. Cherepkova, A.I. Zhernovoi. Russian Journal of Applied Chemistry. 89 (4), 535 (2016). Crossref
12. A.V. Anupama, V. Rathod, V.M. Jali, B. Sahoo. Journal of Alloys and Compounds. 728, 1091 (2017). Crossref

13. K.D. Martinson, I.A. Cherepkova, V.V. Sokolov. Glass Physics and Chemistry. 44 (1), 21 (2018). Crossref
14. R. Guo, Z. Yu, Y. Yang, X. Jiang, K. Sun, C. Wu, Z. Xu, Z. Lan. Journal of Alloys and Compounds. 589, 1 (2014). Crossref
15. K.D. Martinson, S.S. Kozyritskaya, I.B. Panteleev, V.I. Popkov. Nanosystems: Physics, Chemistry, Mathematics. 10 (3), 313 (2019). Crossref
16. S.E. Shirsath, R.H. Kadam, A.S. Gaikwad, A. Ghasemi, A. Morisako. Journal of Magnetic Materials. 323, 3104 (2011). Crossref
17. M. Tabuchi, K. Ado, H. Sakaebe, C. Masquelier, H. Kageyama, O. Nakamura. Solid State Ionics. 79, 220 (1995). Crossref
18. V.V. Zvereva, V.I. Popkov. Ceramics International. 45, 1380 (2019). Crossref
19. N.S.A. Puad, A.F.M. Fadzil, R. Yusof, N. Kamarulzaman. AIP Conference Proceedings. 1217, 370 (2010). Crossref
20. Y. Lin, J. Dong, J. Dai, J. Wang, H. Yang, H. Yang, H. Zong. Inorganic Chemistry. 56 (24), 14960 (2017). Crossref
21. I.S. Kondrashkova, K.D. Martinson, N.V. Zakharova, V.I. Popkov. Russian Journal of General Chemistry. 88 (12), 2465 (2018). Crossref
22. P. Naderi, S.M. Masoudpanah, S. Alamolhoda. Applied Physics A. 123, 702 (2017). Crossref
23. K.D. Martinson, I.S. Kondrashkova, V.I. Popkov. Russian Journal of Applied Chemistry. 90 (8), 1214 (2017). Crossref
24. A.S. Mukasyan, P. Dinka. International Journal of Self-Propagating High-Temperature Synthesis. 16 (1), 23 (2007). Crossref
25. A. Bachina, V.A. Ivanov, V.I. Popkov. Nanosystems: Physics, Chemistry, Mathematics. 8 (5), 647 (2017). Crossref
26. R.Y.S. Zampiva, C.G. Kaufmann, A.K. Alves, C.P. Bergmann. FME Transactions. 46 (2), 157 (2018).Crossref
27. H. Wu, H. Li, G. Sun, S. Ma, X. Yang. Journal of Materials Chemistry C. 3, 5456 (2015). Crossref
28. E.N. Lysenko, A.V. Malysheva, V.A. Vlasov, E.V. Nikolaev, A.P. Surzhikov. Journal of Thermal Analysis and Calorimetry. 134 (1), 127 (2018). Crossref
29. Y.M. Dai, Y.F. Wang, C.C. Chen. Catalyst Communications. 106, 20 (2018). Crossref
30. X. Wang, L. Gao, L. Li, H. Zheng, Z. Zhang, W. Yu, Y. Qian. Nanotechnology. 16, 2677 (2005). Crossref